Inter-pixel Crosstalk in Auger-Suppressed Dense Infrared Detectors

Inter-pixel Crosstalk in Auger-Suppressed Dense Infrared Detectors

M. Vallone[1], **M. Goano**[1], **F. Bertazzi**[1], **G. Ghione**[1], **S. Hanna**[2], **D. Eich**[2], **and H. Figgemeier**[2]

[1]Dipartimento di Elettronica e Telecomunicazioni, Politecnico di Torino
Corso Duca degli Abruzzi 24, Torino 10129, Italy
[2]AIM Infrarot-Module GmbH, Theresienstraße 2, D-74072 Heilbronn, Germany

Abstract— We simulated the optical and electrical response of a planar HgCdTe 5×5 pixel miniarray with $5\,\mu$m-wide square pixels, illuminated by narrow Gaussian beams. The compositional grading of the HgCdTe absorber required particular techniques to obtain combined three-dimensional, realistic full-wave electromagnetic and electrical simulations. The simulation results suggest that, by avoiding quasi-neutral regions in the detector's absorber through majority carriers depletion, not only the Auger contribution to dark current results suppressed, but also the inter-pixel crosstalk due to the diffusion of photogenerated carriers is significantly reduced.

1. INTRODUCTION

The II-VI alloy HgCdTe is one of the most versatile materials for the realization of large format infrared (IR) focal plane arrays (FPAs) [1]. Recently, cost and performance considerations have motivated a significant effort aimed at developing diffraction-limited operation. This consists in fabricating FPAs with pixel pitch $d \approx F\lambda/2$ (Nyquist criterion) [2], where λ is the wavelength of the illuminating radiation, and F is the focal ratio of the camera objective. Hence, for $F = 1$, the pixel pitch d is of the order of $3 \div 5\,\mu$m and $5 \div 6\,\mu$m, respectively, for mid wavelength (MWIR, $\lambda \in [3, 5]\,\mu$m) and long wavelength (LWIR, $\lambda \in [8, 14]\,\mu$m) detectors [3, 4].

On the other hand, expensive cryogenic cooling of HgCdTe IR detectors is typically needed in order to decrease dark current and noise arising from several mechanisms associated with the material narrow band gap [5]. The possibility to operate at room temperature — or at least to reduce the cooling requirement — triggered large efforts in developing novel approaches towards the development of High Operating Temperature (HOT) detectors [6, 7]. Adopting nBn structures [8, 9] or suppressing the Auger recombination rate by fully carrier-depleting Double Layer Planar Heterostructures (DLPH), it is possible to reduce the fundamental detector's limitation given by the dark diffusion current [1, 10]. HOT operability and dense FPAs (large format, diffraction limited FPAs) should provide the advantage of smaller volume, lower weight, optimal spatial resolution, and potentially lower cost.

However, since the minority carrier diffusion length L_d in HgCdTe is much longer (typically tens of micrometers) that d, IR planar FPAs detectors with subwavelength pixel pitch may be prone to the diffusive inter-pixel crosstalk [11], a deleterious effect due to carriers that, photogenerated in the quasi-neutral region of a pixel, diffuse to neighboring ones [2, 11]. After having verified the expected dark current reduction due to Auger-suppression [10] even for low values of reverse bias, the present work investigates the approach of reducing the extension of quasi-neutral regions in a DLPH detector as a method to cut down the inter-pixel crosstalk due to carrier diffusion, as already described for simpler p-ν-n homojunction FPAs [12].

In Section 2 the detector is described as case study, and Section 3 outlines the simulation method. Simulated spectral quantum efficiency (QE) and inter-pixel crosstalk are shown and discussed in Section 4, and Section 5 summarizes the main outcomes.

2. PHOTODETECTOR STRUCTURE

We designed a planar 5×5 pixels miniarray with $5\,\mu$m-wide square pixels (Fig. 1). Composition and doping profiles are a small modification of a literature example [13]: above a CdTe substrate, a wide-bandgap n-$Hg_{0.6}Cd_{0.4}Te$ layer (buffer) was considered, donor-doped with concentration $N_D = 5 \times 10^{17}\,\mathrm{cm}^{-3}$. It is followed by a $5\,\mu$m thick, low donor-doped ($N_\mathrm{D} = 1 \times 10^{14}\,\mathrm{cm}^{-3}$), narrow-bandgap $Hg_{1-x}Cd_xTe$ absorber layer with linearly graded composition ($0.19 \le x \le 0.25$ according to Fig. 1(b)), and by another wide-bandgap $Hg_{0.6}Cd_{0.4}Te$ cap layer, with the same low donor

concentration. The *n*-*p* photodiode junction was defined by simulating an ion implantation, yielding an error-function-shaped acceptor density N_A ranging from $5\times10^{16}\,\mathrm{cm}^{-3}$ just below the bias contact to virtually zero at the *n*-*p* junction in about 2.5 µm. Above this heterostructure, a 0.3 µm thick CdTe passivation layer covers all the miniarray. In order to increase realism two 0.5 µm thick transition regions with linear compositional grading connect the two high-E_g regions to the low-E_g absorber layer (where E_g is the bandgap). The absorber cutoff wavelength λ_c (defined in micrometers as $\lambda_c = 1.24/E_g$, where E_g is in eV) varies along the growth direction z between 6.9 µm and 14.2 µm at $T = 140\,\mathrm{K}$ (and between 6.0 µm and 10.6 µm at $T = 230\,\mathrm{K}$), making the detector to effectively absorb IR radiation from MWIR to LWIR bands. The bias contact is a 4 µm × 4 µm square metallic layer above the passivation, connected to the *p*-doped region via a circular hole with radius of 1 µm through the CdTe layer (Fig. 1(c)).

3. SIMULATION METHOD

The current in dark I_{dark} and under illumination I were obtained in the drift-diffusion approximation, where the Poisson's and the continuity equations for the electron and hole current densities $J_{n,p}$ were self-consistently solved as outlined in [2, 14, 15]. The photogeneration rate G_{opt} due to illumination enters in the continuity equations as a source term, and the photocurrent I_{ph} and quantum efficiency QE follow as $I_{\mathrm{ph}} = I - I_{\mathrm{dark}}$ and $\mathrm{QE} = I_{\mathrm{ph}}/(qN_{\mathrm{phot}})$ respectively, where q is the elementary charge and N_{phot} is the photon flux impinging the illuminated face. The geometry, doping and composition profiles were defined employing the Sentaurus three-dimensional (3D) numerical simulator by Synopsys [16], also used to perform the electrical simulations. The detector in Fig. 1 was discretized into $\approx 9.5\times10^5$ elements with a meshing tool which generates a denser grid in regions where gradients of current density, electric field, free charge density and material composition are present. The HgCdTe properties were described through the models reported in [2], taking into account the composition, doping, and temperature dependence of the HgCdTe alloy. The Shockley-Read-Hall (SRH) recombination processes were modeled as in [17, 18] considering a lifetime around 100 µs. Fermi-Dirac statistics and incomplete dopant ionization were taken into account, with activation energies for HgCdTe alloys estimated according to [19, 20]. Electric contacts were treated as Ohmic with zero resistance, where charge neutrality and equilibrium were assumed. Ideal Neumann boundary conditions (BCs) were applied to the outer boundaries of the array, and the drift-diffusion equations were solved by the Finite Box method.

3.1. Simulations in Dark

Simulations have been done considering Auger and SRH as generation-recombination (GR) processes, neglecting instead radiative processes. Extensive discussion about this important point can be found in [21] and references therein. At the moderate reverse bias considered in the present work (not higher than $-0.5\,\mathrm{V}$), the band-to-band, trap-assisted tunneling and impact ionization may be safely neglected [18, 22, 23].

In Figs. 2(a), (b) the electron and hole density n, p and the intrinsic density n_i are shown in dark for $T = 140\,\mathrm{K}$ in reverse bias ($-0.1\,\mathrm{V}$ and $-0.5\,\mathrm{V}$). The effect of carrier depletion is well visible: even for reverse bias equal to $-0.1\,\mathrm{V}$, n and p in the absorber ($5\,\mu\mathrm{m} \le z \le 10\,\mu\mathrm{m}$) are below the intrinsic density, but as soon as reverse bias increases to $-0.5\,\mathrm{V}$, their values drop towards very low values (except in the lower half detector, $5\,\mu\mathrm{m} \le z \le 7.5\,\mu\mathrm{m}$).

A consequence of this behavior is the suppression of the Auger generation, as visible in Figs. 3(a), (b), particularly effective where the electric field is higher, see Fig. 4(a). Nevertheless, as supposed the electric field does not reach values as high as required to trigger significant impact ionization and tunneling generation [18, 24]. The increase of electric field with increasing reverse bias makes the simulated I_{dark} to *decrease* progressively and considerably with increasing V_{bias} (after a maximum value is reached around $-0.05\,\mathrm{V}$), as shown in Fig. 4(b) for $T = 140\,\mathrm{K}$ and $T = 230\,\mathrm{K}$, confirming a behavior obtained by other groups [10, 13] for similar carrier-depleted absorbers.

3.2. Combined Electromagnetic and Electrical Simulations

In order to investigate inter-pixel crosstalk, we simulated the photoresponse to a narrow Gaussian beam illuminating the miniarray from below (see Fig. 5(a)). The beam waist (its radius is $w_0 \approx 2.5\,\mu\mathrm{m}$) lies on the 1 µm thick substrate's lower face, and the beam axis is orthogonal to the detector horizontal plane xy and centered on the miniarray's central pixel (CP). Very generally, with reference to Figs. 5(a), (b) the inter-pixel crosstalk is the photoresponse of a neighboring pixel to a beam illuminating the CP. Considering the LWIR band, it is $\lambda > d$, and the compositional grading makes the photogeneration to take place mostly in the absorber region closest to the bias

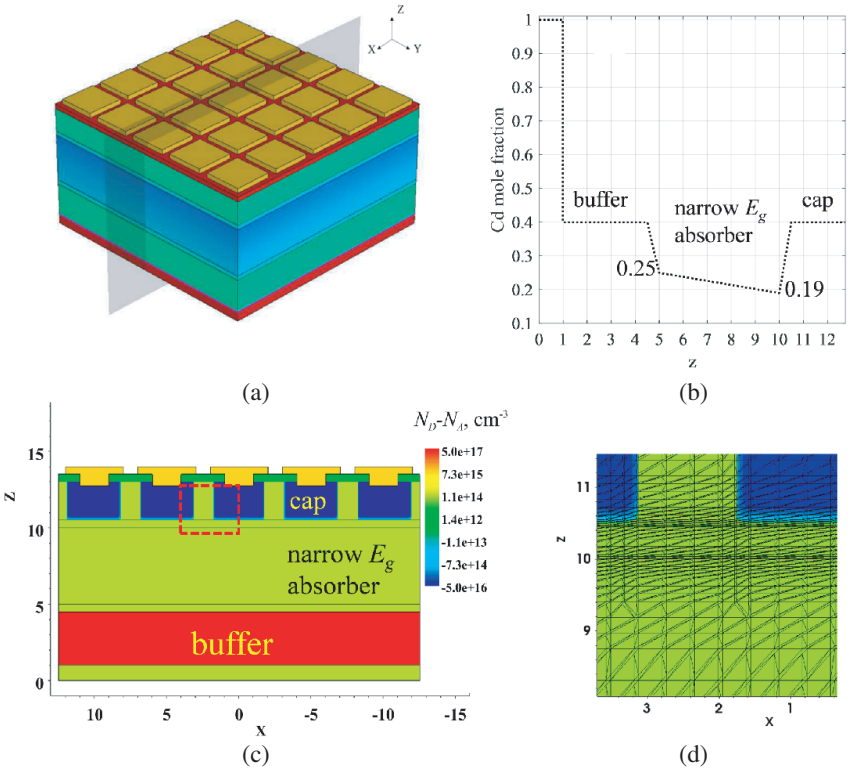

Figure 1. (a) The 3D miniarray. In panel (b), the Cd mole fraction x of $Hg_{1-x}Cd_xTe$ along z and in (c) the dopant distribution across a two-dimensional section are shown. A detail of the electrical mesh in shown in panel (d).

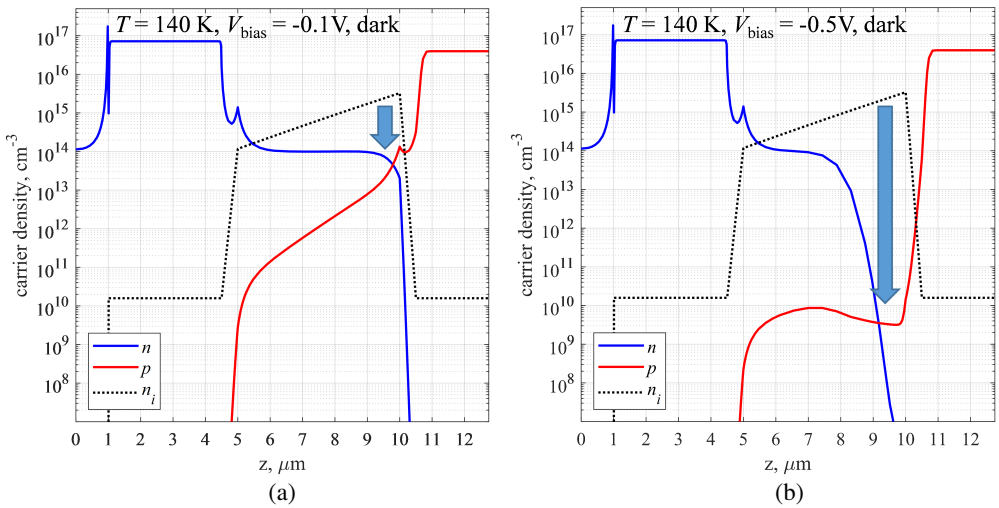

Figure 2. Electron and hole density n, p and intrinsic density n_i in dark for $T = 140\,\mathrm{K}$, in reverse bias ($-0.1\,\mathrm{V}$ and $-0.5\,\mathrm{V}$, respectively in panels (a) and (b)).

contact. There, the narrower E_g increases the minority carriers mobility (see [2], Table 1), in principle favoring the diffusion. The presence of a moderately high, z-oriented electric field in this region helps in sweeping out the photogenerated carriers, before they diffuse laterally (diffusive contribution to the inter-pixel crosstalk, see Section 4).

The choice of a compositional grading is not an issue for electrical simulations, since the considered simulator reads the nominal HgCdTe composition profile at each point of the electrical grid, locally evaluating the electrical properties of the material without any problem. Conversely, the solution of the electromagnetic problem for detectors with arbitrary composition profile may not be straighforward, since not all simulators directly manage a compositional grading, requiring to define the detector geometry as a stack of layers each with uniform optical properties. Thus, we

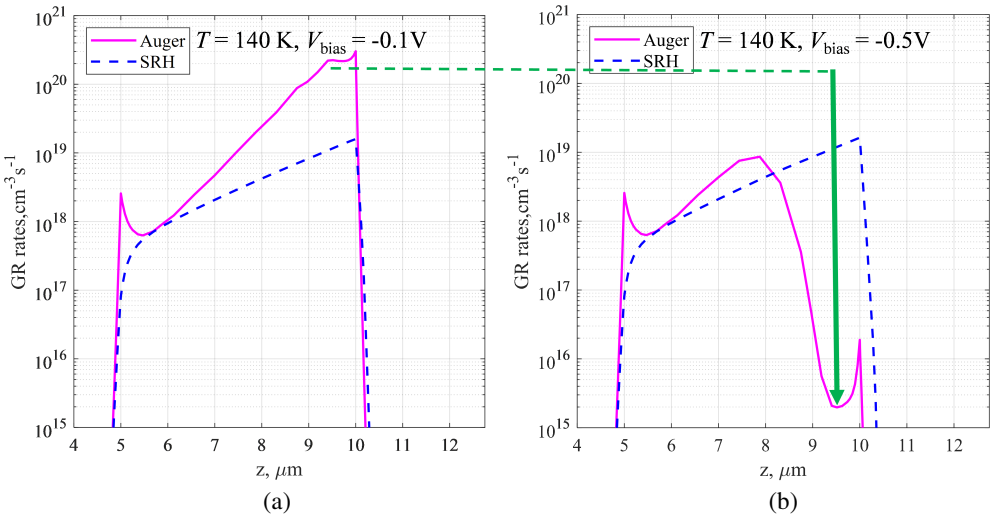

Figure 3. The Auger and SRH net GR rates for $T = 140\,\mathrm{K}$, in reverse bias ($-0.1\,\mathrm{V}$ and $-0.5\,\mathrm{V}$, respectively in panels (a) and (b)).

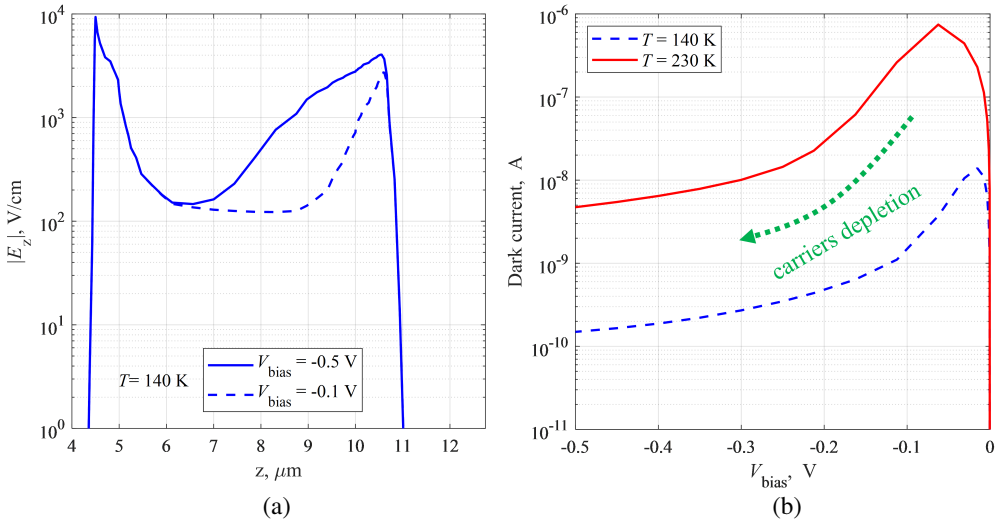

Figure 4. (a) The z-component of the electric field magnitude for $T = 140\,\mathrm{K}$, in reverse bias ($-0.1\,\mathrm{V}$ and $-0.5\,\mathrm{V}$). (b) The simulated dark current, for $T = 140\,\mathrm{K}$ and $T = 230\,\mathrm{K}$.

sampled the absorber's and the transition regions' composition profiles [25], converting them to staircases of $N = 30$ sublayers, each with uniform value for the complex refractive index $n_r + i\kappa$ according to the sublayer's HgCdTe composition ([2], Table 1), as shown in Figs. 5(b)–(d). With this approach, the EMW commercial simulator [16] was able to solve the electromagnetic problem by a full-wave approach, according to the Finite Differences Time Domain (FDTD) method [26]. The solution of the Maxwell's equations yields the distribution of the absorbed photon density in the miniarray $A_{\mathrm{opt}} = 1/(2h\nu)\sigma|\vec{E}|^2$, which takes into account the back-reflections and interference effects not addressed by simpler methods based on the Beer's law [27] (here $h\nu$ is the photon energy, $\vec{E}$ the electric field, $\sigma = n_r\alpha/(\mu_0 c)$ is the electric conductivity, $\alpha = 4\pi\kappa/\lambda$ is the absorption coefficient, μ_0 the vacuum magnetic permeability, and c is the speed of light in vacuum).

4. RESULTS AND COMMENTS

The optical generation rate distribution G_{opt} into the pixel due to interband optical absorption is given by $G_{\mathrm{opt}} = \eta A_{\mathrm{opt}}$, where the quantum yield η, defined as the fraction of absorbed photons which are converted to photogenerated electron-hole pairs, was assumed to be unitary. As an

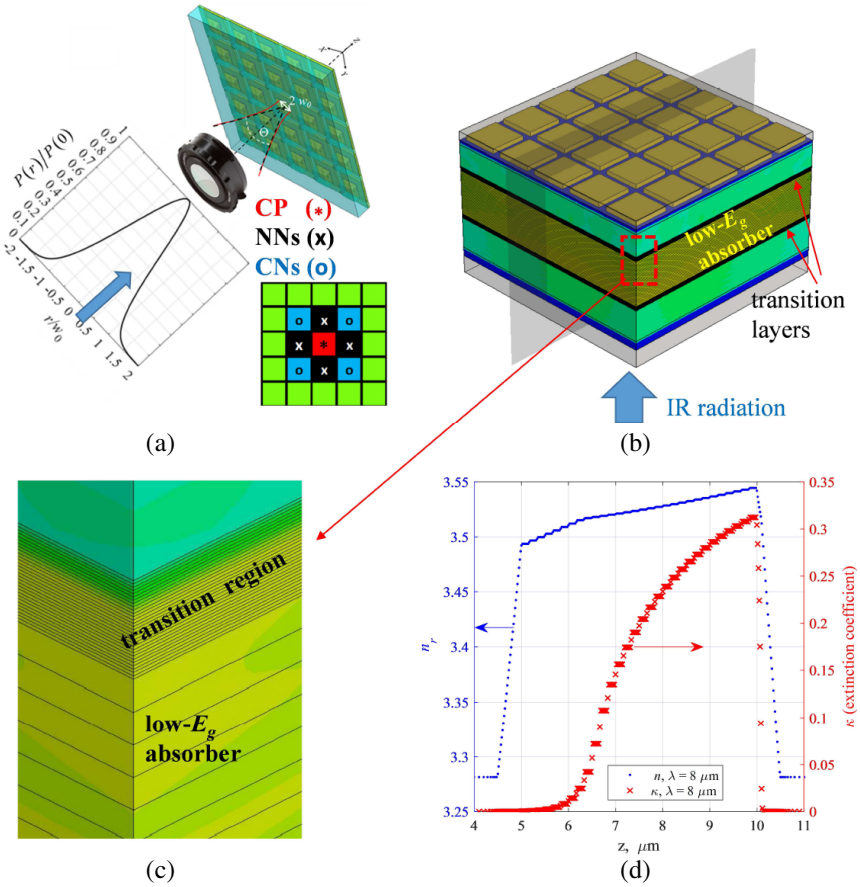

Figure 5. (a) The miniarray illumination, with the CP, NNs and CNs pixel definitions, (b) the discretization of the 3D absorber and transition regions into N sublayers, each with uniform n_r and κ according to the HgCdTe composition, also shown along a xz cutplane (c) and along a cutline (d) along z, for one of the considered wavelengths.

example, in Fig. 6 $A_{\rm opt}$ is shown for some values of λ, along xz-cutplanes and along a z-cutline at center pixel. When inserted in the drift-diffusion equations after having applied the same reverse bias $V_{\rm bias}$ to all the pixels, the photocurrent collected by each of them allows to study several important figures of merit. Fig. 7 shows the spectral QE and the inter-pixel crosstalk at $T = 140\,{\rm K}$ for $V_{\rm bias} = -0.1\,{\rm V}$ and $-0.5\,{\rm V}$ for the described illumination, where the definitions for the "total" $\mathcal{C}_{NNs}$, "optical" $\mathcal{O}_{NNs}$ and "diffusive" $\mathcal{D}_{NNs}$ contributions to the crosstalk

$$\mathcal{C}_{NNs} = \frac{I_{ph,\,NNs}}{I_{ph,\,CP}}, \quad \mathcal{O}_{NNs} = \frac{\int_{V_{NNs}} G(x,y,z)\,dx\,dy\,dz}{\int_{V_{CP}} G(x,y,z)\,dx\,dy\,dz}, \quad \mathcal{D}_{NNs} \approx \mathcal{C}_{NNs} - \mathcal{O}_{NNs} \tag{1}$$

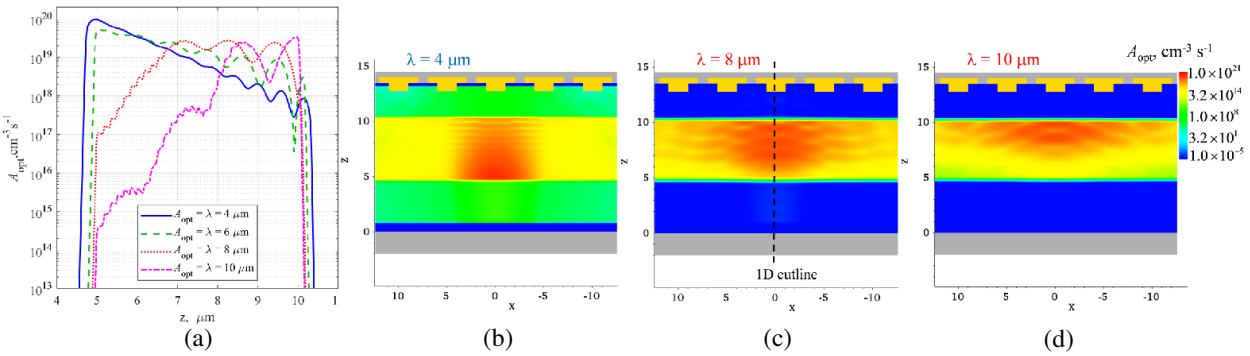

Figure 6. (a) The $A_{\rm opt}$ distribution for 4 values of λ along a z-cutline at center pixel. In panels (b)–(d), $A_{\rm opt}$ is shown along xz-cutplanes at center pixel, for $\lambda = 4, 8, 10\,\mu$m (the colorbar holds for all the three panels).

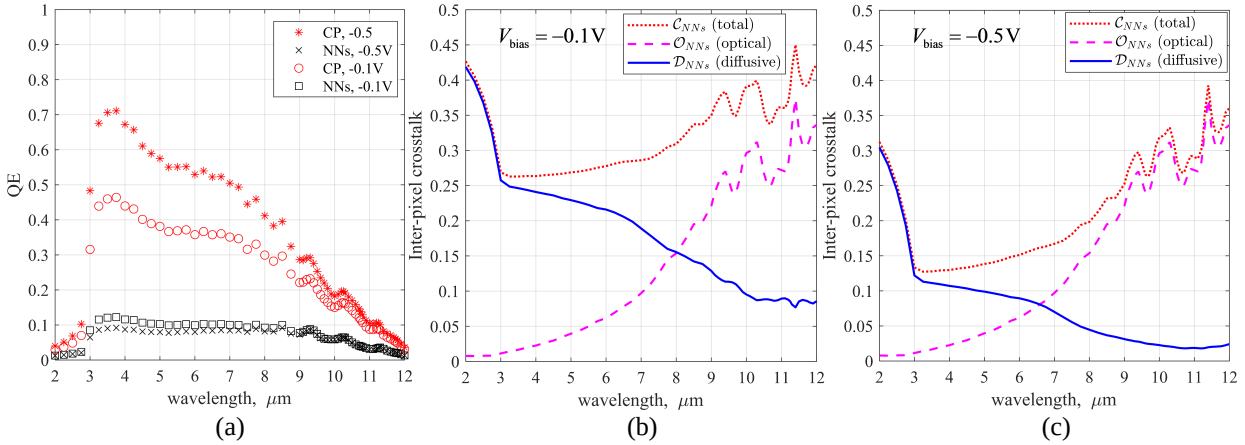

Figure 7. (a) The CP and NNs spectral QE for the described Gaussian beam illumination centered on the CP, for $T = 140\,\mathrm{K}$ and $V_{\mathrm{bias}} = -0.1\,\mathrm{V}$ and $-0.5\,\mathrm{V}$. For the same temperature, the "total", "optical" and "diffusive" inter-pixel crosstalk (adimensional ratios) are shown for $V_{\mathrm{bias}} = -0.1\,\mathrm{V}$ (panel (b)) and $-0.5\,\mathrm{V}$ (panel (c)).

have been introduced and extensively discussed in [12] (V_{CP} and V_{NNs} are the CP and NNs pixel volumes). We showed that by increasing the reverse bias from $-0.1\,\mathrm{V}$ to $-0.5\,\mathrm{V}$, the carrier depletion in the absorber increases significantly (Figs. 2(a), (b)). As a result, the ensuing increase of electric field throughout the absorber (Fig. 4(a)) makes a larger fraction of photogenerated carriers to drift towards the CP contact, before they diffuse laterally: this is pretty apparent comparing the blue solid lines in Figs. 7(b), (c). The resulting capability to curtail the inter-pixel "diffusive" crosstalk at moderate reverse bias is an additional advantage — beside the Auger suppression — of such detectors.

5. CONCLUSIONS AND FUTURE WORK

Realistic three-dimensional full-wave electromagnetic and electrical simulations were obtained for a planar HgCdTe FPA with graded composition, illuminated by narrow Gaussian beam. The moderate electrical field in the absorber ensues from the depletion of the majority carriers, and it is enough to make most of the carriers photogenerated in the central pixel to drift and be collected by its electrical contact, before they diffuse towards the neighboring pixels. Therefore, the "diffusive" crosstalk is cut down considerably even at moderate reverse bias. The outlined method will be employed in a future work to explore the effect of different doping and composition profiles, absorber thickness, bias voltage, also considering broadband, blackbody optical sources with different spectral temperature.

REFERENCES

1. Kinch, M. A., "The future of infrared; III-Vs or HgCdTe?" *J. Electron. Mater.*, Vol. 44, No. 9, 2969–2976, 2015.
2. Vallone, M., M. Goano, F. Bertazzi, G. Ghione, W. Schirmacher, S. Hanna, and H. Figgemeier, "Simulation of small-pitch HgCdTe photodetectors," *J. Electron. Mater.*, Vol. 46, No. 9, 5458–5470, 2017.
3. Driggers, R. G., R. Vollmerhausen, J. Reynolds, J. Fanning, and G. C. Holst, "Infrared detector size: how low should you go?" *Opt. Eng.*, Vol. 51, No. 6, 063202, 2012.
4. Rogalski, A., Martyniuk, and M. Kopytko, "Challenges of small-pixel infrared detectors: a review," *Rep. Prog. Phys.*, Vol. 79, No. 4, 046501, 2016.
5. Kinch, M. A., "Fundamental physics of infrared detector materials," *J. Electron. Mater.*, Vol. 29, No. 6, 809–817, 2000.
6. Ashley, T. and C. T. Elliott, "Model for minority carrier lifetimes in doped HgCdTe," *Electron. Lett.*, Vol. 21, No. 10, 451–452, 1985.
7. Martyniuk, and A. Rogalski, "HOT infrared photodetectors," *Opto-Electron. Rev.*, Vol. 21, No. 2, 239–257, 2013.

8. Maimon, S. and G. W. Wicks, "nBn detector, an infrared detector with reduced dark current and higher operating temperature," *Appl. Phys. Lett.*, Vol. 89, No. 15, 151109, 2006.
9. Itsuno, A. M., J. D. Phillips, and S. Velicu, "Mid-wave infrared HgCdTe nBn photodetector," *Appl. Phys. Lett.*, Vol. 100, No. 16, 161102; *Appl. Phys. Rev.*, 2012.
10. Schuster, J., R. DeWames, and S. Wijewarnasurya, "Dark currents in a fully-depleted LWIR HgCdTe P-on-n heterojunction: analytical and numerical simulations," *J. Electron. Mater.*, Vol. 46, No. 11, 6295–6305, 2017.
11. Pinkie, B. and E. Bellotti, "Numerical simulation of spatial and spectral crosstalk in two-color MWIR/LWIR HgCdTe infrared detector arrays," *J. Electron. Mater.*, Vol. 42, No. 11, 3080–3089, 2013.
12. Vallone, M., M. Goano, F. Bertazzi, G. Ghione, S. Hanna, D. Eich, and H. Figgemeier, "Diffusive-probabilistic model for inter-pixel crosstalk in HgCdTe focal plane arrays," *IEEE J. Electron Devices Soc.*, Vol. 6, No. 1, 664–673, 2018.
13. Rogalski, A., M. Kopytko, and Martyniuk, "Performance prediction of p-i-n HgCdTe long-wavelength infrared HOT photodiodes," *Appl. Opt.*, Vol. 57, No. 18, D11–D18, 2018.
14. Vallone, M., M. Goano, F. Bertazzi, G. Ghione, W. Schirmacher, S. Hanna, and H. Figgemeier, "Comparing FDTD and ray tracing models in the numerical simulation of HgCdTe LWIR photodetectors," *J. Electron. Mater.*, Vol. 45, No. 9, 4524–4531, 2016.
15. Vallone, M., A. Palmieri, M. Calciati, F. Bertazzi, F. Cappelluti, G. Ghione, M. Goano, M. Bahl, E. Heller, R. Scarmozzino, S. Hanna, D. Eich, and H. Figgemeier, "Non-monochromatic 3D optical simulation of HgCdTe focal plane arrays," *J. Electron. Mater.*, Vol. 47, No. 10, 5742–5751, 2018.
16. Sentaurus Device User Guide, Version M-2017.09, Synopsys, Inc., Mountain View, CA, Sept. 2017.
17. Sze, S. M. and K. K. Ng, *Physics of Semiconductor Devices*, 3rd Edition, John Wiley & Sons, Hoboken, NJ, 2007.
18. Vallone, M., M. Mandurrino, M. Goano, F. Bertazzi, G. Ghione, W. Schirmacher, S. Hanna, and H. Figgemeier, "Numerical modeling of SRH and tunneling mechanisms in high-operating-temperature MWIR HgCdTe photodetectors," *J. Electron. Mater.*, Vol. 44, No. 9, 3056–3063, 2015.
19. Rogalski, A., *Infrared Detectors*, 2nd Edition, CRC Press, Boca Raton, FL, 2011.
20. Capper, and J. Garland, Eds., *Mercury Cadmium Telluride, Growth, Properties and Applications*, John Wiley & Sons, Chichester, UK, 2011.
21. Kopytko, M., K. Jóźwikowski, Martyniuk, and A. Rogalski, "Photon recycling effect in small pixel p-i-n HgCdTe long wavelength infrared photodiodes," *Infrared Phys. Tech.*, Vol. 97, 38–42, 2019.
22. Mandurrino, M., G. Verzellesi, M. Goano, M. Vallone, F. Bertazzi, G. Ghione, M. Meneghini, G. Meneghesso, and E. Zanoni, "Trap-assisted tunneling in InGaN/GaN LEDs: experiments and physics-based simulation," *14th International Conference on Numerical Simulation of Optoelectronic Devices (NUSOD 2014)*, 13–14, Palma de Mallorca, Spain, Sept. 2014.
23. Mandurrino, M., M. Goano, M. Vallone, F. Bertazzi, G. Ghione, G. Verzellesi, M. Meneghini, G. Meneghesso, and E. Zanoni, "Semiclassical simulation of trap-assisted tunneling in GaN-based light-emitting diodes," *J. Comp. Electron.*, Vol. 14, No. 2, 444–455, Jun. 2015.
24. Rothman, J., L. Mollard, S. Goût, L. Bonnefond, and J. Wlassow, "History-dependent impact ionization theory applied to HgCdTe e-APDs," *J. Electron. Mater.*, Vol. 40, No. 8, 1757–1768, 2011.
25. Vallone, M., M. Goano, F. Bertazzi, G. Ghione, S. Hanna, D. Eich, and H. Figgemeier, "FDTD simulation of compositionally graded HgCdTe photodetectors," *Infrared Phys. Tech.*, Vol. 97, 203–209, 2019.
26. Berenger, J.-P., "A perfectly matched layer for the absorption of electromagnetic waves," *J. Comp. Phys.*, Vol. 114, No. 2, 185–200, 1994.
27. Born, M. and E. Wolf, *Principles of Optics. Electromagnetic Theory of Propagation, Interference and Diffraction of Light*, 7th Edition, Cambridge University Press, Cambridge, UK, 1999.